Implementation and Testing of Radar Data Assimilation Capabilities Within the Joint Effort for Data Assimilation Integration Framework With Ensemble Transformation Kalman Filter Coupled With FV3-LAM Model

Jun Park[1] [ID]**, Ming Xue[1,2]** [ID]**, and Chengsi Liu[1]** [ID]

[1]Center for Analysis and Prediction of Storms, University of Oklahoma, Norman, OK, USA, [2]School of Meteorology, University of Oklahoma, Norman, OK, USA

Abstract Capabilities to directly assimilate radar data are implemented within the local ensemble transform Kalman filter (LETKF) and the gain-form LETKF (LGETKF) algorithms of the Joint Effort for Data assimilation Integration (JEDI) system. The capabilities are evaluated for the analysis and forecast of a severe convection case of 20 May 2019 in the Southern Great Plains using the limited area model version of the FV3 dynamical core (FV3-LAM) from a recent release for Short-Range Weather Application (SRW App). The LETKF and LGETKF implementations are shown to produce analyses and short-range forecasts comparable to those using the ensemble square-root Kalman Filter (EnSRF) within the Gridpoint Statistical Interpolation (GSI) framework used by current NCEP operational models. In addition, LGETKF retaining only 60% variances for model-space vertical localization performs similarly to LGETKF retaining 99% of variance and LETKF using observation error-based vertical localization. JEDI LETKF shows better parallel scalability than LGETKF and GSI EnSRF.

Plain Language Summary The JEDI data assimilation (DA) framework under development will be used by all operational forecasting systems of the U.S. National Weather Service, including the Rapid Refresh Forecast System based on FV3, a dynamic core chosen for next-generation NWS forecasting systems. In this study, we implemented radar DA capabilities into the JEDI with two local ensemble transform Kalman filter (LETKF) algorithms coupled with limited-area FV3. Analyses and forecasts with radar DA better match radar reflectivity and radial velocity observations than forecasts without radar DA during the assimilation period. Three-hour forecasts of precipitation, reflectivity, and updraft rotation show skills comparable to a DA experiment using the ensemble square-root Kalman filter within the more mature GSI DA system. In addition, the new gain-form LETKF, which has not been applied to radar DA before, performs quite well, although it is computationally more expensive than the regular LETKF. This work paves the way for using JEDI to assimilate radar data in operational forecasting systems.

1. Introduction

The Unified Forecast System (UFS; https://ufscommunity.org) based on the Finite-Volume Cubed-Sphere (FV3) dynamical core (Harris et al., 2021; Lin, 2004; Putman & Lin, 2007) is being developed as a next-generation modeling framework for all operational forecasting of the U.S. National Weather Service (NWS) at all scales, and for community research in earth system modeling (Schneider et al., 2017). One of the important applications of UFS is the Rapid Refresh Forecast System (RRFS) for regional ensemble forecasting at a ~3 km convection-allowing resolution (Kinter et al., 2020). In the meanwhile, the Joint Effort in Data assimilation Integration (JEDI, Trémolet & Auligné, 2020) framework is being developed as the next-generation DA infrastructure for UFS to replace the Gridpoint Statistical Interpolation (GSI, Kleist et al., 2009) data assimilation (DA) system that is currently used by all NWS operational forecast models.

The first public release of JEDI (https://www.jcsda.org/jcsda-project-jedi) supporting FV3 dynamical core became available in October 2020, and JEDI supports both variational and ensemble DA algorithms. The prototype JEDI has been tested for several applications with global models. For example, JEDI 3-dimensional variational (3DVar) DA has been used to produce interim Marine Reanalysis data over a 40 year period (https://registry.opendata. aws/noaa-ufs-marinereanalysis). Baker et al. (2022) showed that the analysis increments and verification metrics

Project Administration: Ming Xue, Chengsi Liu
Software: Jun Park
Supervision: Ming Xue, Chengsi Liu
Validation: Jun Park
Visualization: Jun Park
Writing – original draft: Jun Park
Writing – review & editing: Ming Xue, Chengsi Liu

against radiosonde data from the JEDI-based 3DVar are comparable to those from the current operational DA system at Naval Research Laboratory for a three-month-long cycling experiment. Huang et al. (2022) demonstrated that JEDI-based pure ensemble-variational (EnVar) DA improved aerosol optical depth forecasts using FV3-based global model. Z. Liu et al. (2022) showed that assimilating all-sky microwave radiance along with conventional observations using JEDI EnVar improved surface and precipitation forecasts in global Model for Prediction Across Scales (MPAS, Skamarock et al., 2012).

Although JEDI also supports the limited area model version of FV3 (FV3-LAM, Black et al., 2021), capabilities to assimilate regional data sets within JEDI for regional applications are still limited. No paper has been formally published testing and evaluating JEDI with FV3-LAM according to our knowledge.

Many studies have been shown positive impacts of assimilating radar data on convective-scale forecasts (e.g., Kain et al., 2010; Stensrud et al., 2013; Sun et al., 2014). Recently, capabilities for directly assimilating radar reflectivity (Z) and radial velocity (V_r) data have been added to the GSI ensemble Kalman filter (EnKF, Evensen, 1994; Evensen, 2003) and hybrid EnVar (Hamill & Snyder, 2000) systems by this research team and the evaluation results are documented in a series of papers (Chen et al., 2021, 2022; Labriola et al., 2021; Li et al., 2022; C. Liu et al., 2022; C. C. Tong et al., 2020). Radar DA capability was not available in JEDI before this work, however. Given that JEDI will replace GSI for regional operational forecasting, it is important to implement and test such capabilities within JEDI.

EnKF is one of the preferred methods for assimilating radar data. With the help of ensemble-derived cross-variable covariances, state variables not directly observed by radar can be updated (e.g., Snyder & Zhang, 2003; M. Tong & Xue, 2005). This is especially important for the analysis and forecasting of convective storms inside which few state variables are directly observed. A variant of EnKF, the ensemble square root Kalman filter (EnSRF, Whitaker & Hamill, 2002) algorithm is commonly used for radar DA studies (Labriola et al., 2020; Xue et al., 2006) and such capabilities have been implemented in the GSI DA system (Labriola et al., 2021; Luo et al., 2022). JEDI implements another variant of EnKF, the Local Ensemble Transform Kalman Filter (LETKF, Hunt et al., 2007) and its variation that uses a gain-form LETKF (LGETKF, Bishop et al., 2017) that does vertical localization in model space instead. The LGETKF has been shown to have advantage for vertically integrated observations such as satellite radiance (Lei et al., 2018). The regular LETKF performs vertical localization using a so-called R-based method that adjusts observation error variances depending on the distance between the observation and grid point being updated (Hunt et al., 2007). R-based method is used for horizontal localization in both LETKF and LGETKF. LGETKF has not been previously used for radar DA according to our knowledge.

In this study, the radar DA capabilities implemented within GSI are re-implemented with the LETKF and LGETKF algorithms of JEDI. The enhanced JEDI system is coupled with the Short-Range Weather Application (SRW App) version 2 release of FV3-LAM and tested with a convective storm case that occurred over the Southern Great Plains of the U.S. The results of analysis and forecast using JEDI LETKF and LGETKF, and GSI EnSRF are compared. In addition, the gain-form vertical localization with different degrees of approximation for computational cost saving is assessed. This study is noval in being the application of LGETKF radar DA, and also being the first time that JEDI is applied to regional convective scale DA. The implementation of radar DA capabilities within JEDI is also an important component of this work.

The rest of this paper is organized as follows. Section 2 briefly describes the convective storm case of 20 May 2019. Section 3 describes the DA experiments and Section 4 discusses and evaluates the experimental results. Section 5 presents a summary and conclusions.

2. Case Overview

The convective storms of 20 May 2019 affected the Southern Great Plains of the U.S. and nearby states including Missouri and Arkansas. An upper-level trough was located over the eastern U.S. and a surface low was situated around the central U.S. at 1800 UTC 20 May 2019 (See Figure S1 in Supporting Information S1). This condition formed favorable conditions for severe weather in the early afternoon, including tornadic supercells that developed rapidly in the east of a dryline along a SW-NE-oriented corridor over Texas, Oklahoma, Kansas, and Missouri through the interactions of topography, warm and moist low-level southerly flows, and the jet stream. The NWS Storm Prediction Center (SPC) issued severe weather warnings, including tornados, thunderstorms,

and floods in those regions, and there were 34 tornadoes in total, many wind and hail reports for that day according to the SPC report.

3. Experimental Design

The FV3-LAM of the UFS SRW App version 2 (UFS Development Team., 2022) is employed as the forecast model. The domain uses the extended Schmidt gnomonic grid with 310×310 horizontal grid points (see Figure S1 in Supporting Information S1) across Texas and Oklahoma with a ~3 km grid spacing and 64 vertical levels. We use the "RRFS_v1_alpha" physics suite with the Thompson microphysics scheme (Thompson et al., 2008) from the Common Community Physics Packages (CCPP, Heinzeller et al., 2022). The initial ensemble is started from the NCEP operational Global Data Assimilation System (GDAS) EnKF analyses at 1800 UTC of 20 May 2019 and the corresponding GDAS 3-hourly ensemble forecasts up to 9 hr provide lateral boundary conditions.

The observed Z from Multi-Radar Multi-Sensor (MRMS, Smith et al., 2016) 3D mosaic data and Level-II V_r data from WSR-88D radars are assimilated. V_r observations are processed using an automatic velocity dealiasing algorithm (Brewster et al., 2005). Observation errors for Z and V_r are assumed to be 5 dBZ and 3 m s^{-1}, respectively. Z and V_r forward operators implemented in GSI (Labriola et al., 2021; C. C. Tong et al., 2020) are migrated into the Unified Forward Operator (UFO) module of JEDI. The Z operator following Jung et al. (2008) is consistent with the Thompson microphysics scheme used. The state variables updated by DA include the 3 wind components u, v, w, temperature T, pressure p, specific humidity q_v, mixing ratios of hydrometeors including cloud water q_c, cloud ice q_i, rain water q_r, snow q_s, graupel q_g, and the total number concentration of rain water q_{nr}.

The radar DA capabilities are implemented in the LETKF and LGETKF of JEDI version 1.1.0 released in June 2021. GSI EnSRF is used as a reference. The covariance localization radii are set to 18 km in the horizontal and 0.7 scale height in logarithmic p in the vertical. Since vertical localization was not available in JEDI LETKF of this JEDI release, we additionally implement an R-based vertical localization (Miyoshi & Yamane, 2007) based on the correlation formulas of Gaspari and Cohn (1999). LGETKF uses a modulation approach to generate an expanded ensemble from the raw ensemble and eigenvectors of the localization matrix. To examine the performance and computational efficiency of LGETKF for radar DA with different factions of retained variance, we conduct LGETKF DA experiments with two fraction values of 0.6 and 0.99, which effectively expand the 40 ensemble members to 280 and 1,080 modulated ensemble members, respectively. For covariance inflation, the relaxation-to-prior-spread (Whitaker & Hamill, 2012) method is used to restore the posterior ensemble spread to 99% of the prior ensemble spread.

For the cycled radar DA and forecast experiments (named EnSRF, LETKF, LGETKF.6, and LGETKF.99), radar observations are assimilated every 15 min from 2300 through 0000 UTC (Figure S2 in Supporting Information S1). The 5-hr 40-member ensemble forecasts initialized from 1800 UTC GDAS analyses serve as the background forecasts at 2300 UTC. Ensemble free forecasts from the final analyses at 0000 UTC are run to 3 hr, following the configuration of the Warn-on-Forecast System (WoFS), emphasizing short-range forecasting of severe weather (Jones et al., 2020; Stensrud et al., 2009; Wheatley et al., 2015). Further, the greatest impact of radar DA tends to be limited to the first few hours of forecast (Kain et al., 2010; Sun et al., 2014). We also continue the spinup ensemble forecasts from 2300 UTC for 4 hr without any DA as a baseline (hereafter, NODA). More information on the experiments can be found in Table S1 and Figure S2 in Supporting Information S1.

4. Results

To evaluate the DA performance during the 60-min DA window, root mean squared innovations (RMSIs) and mean innovations of background forecasts and analyses of Z and V_r are calculated against corresponding observations and shown in Figure 1. Compared to NODA, all DA experiments have much lower forecast RMSIs and biases for both Z and V_r after the first cycle. The RMSIs of forecast and analyzed Z are continually reduced through the DA cycles with the reduction being largest in the first cycle (Figures 1a and 1b). The RMSIs of V_r remain at a similar level after large reduction in the first cycle, and the analysis RMSIs are around 2.6 m s^{-1} while the background forecast RMSIs are around 4.7 m s^{-1} (Figures 1c and 1d). The forecast and analysis RMSIs of Z from LETKF are slightly higher than those of EnSRF in later cycles but both are evidently lower than those of LGETKF (Figures 1a and 1b), suggesting that the vertical localization algorithm makes more difference (LETKF vs. LGETKF) than the ensemble filter algorithm difference (LETKF vs. EnSRF). However, for V_r, the forecast
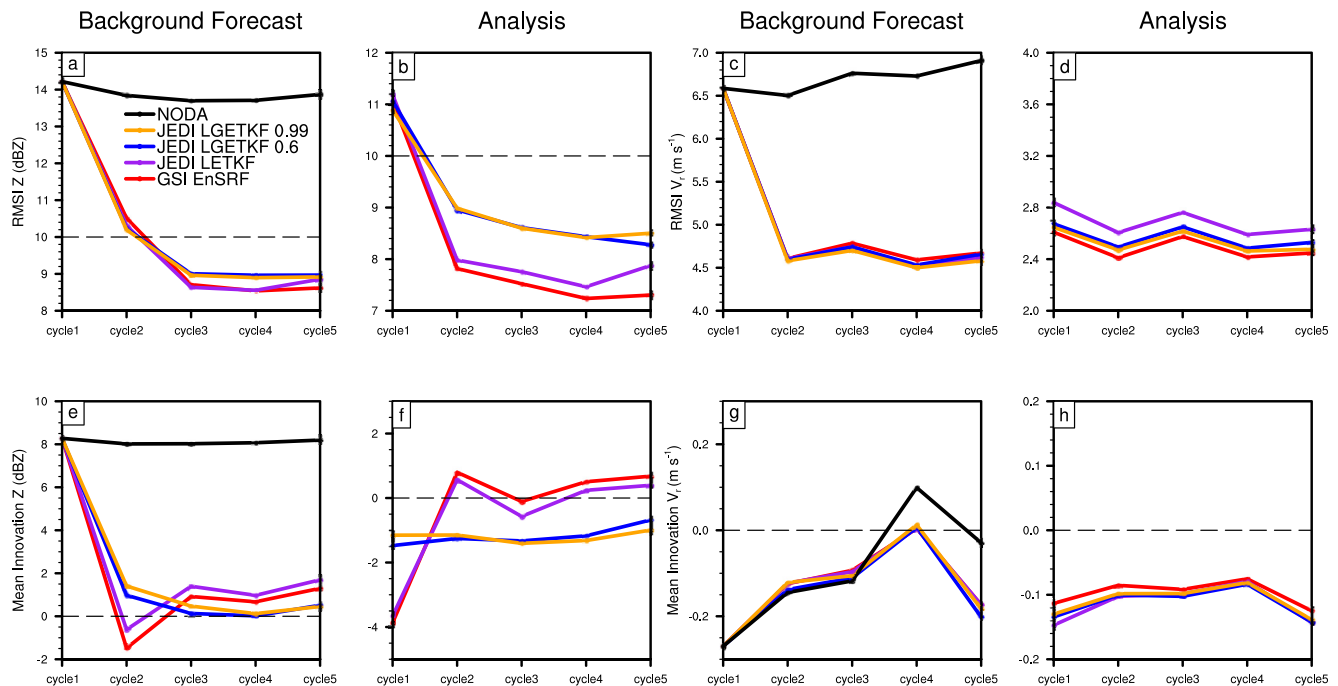
Figure 1. Innovation statistics from ensemble mean for the five experiments during the DA cycles. Top row: Root-mean squared innovations (RMSIs) of reflectivity Z forecasts (a) and analyses (b), and of radial velocity V_r forecasts (c) and analyses (d). Bottom row: Mean innovations or mean biases of Z forecasts (e) and analyses (f) and of V_r forecasts (g) and analysis (h). For Z, statistics are only computed where either observed or simulated reflectivity exceeds 15 dBZ, following C. C. Tong et al. (2020).

RMSIs from different experiments are almost identical (Figure 1c) while the analysis RMSIs of LETKF are slightly higher than those of other experiments (Figure 1d). It is possible that the linear observation operator of V_r reduces the differences among the algorithms.

The mean innovation (observation minus background) of forecast reflectivity at the first analysis cycle (Figure 1e) is largely positive (∼8 dBZ), indicating significant low bias in predicted reflectivity at this time. The forecast reflectivity from NODA remains much lower than observations and analyses of DA experiments at the final analysis time (Figure S3b in Supporting Information S1). The analysis mean innovations of EnSRF and LETKF are close to zero after the first DA cycle while those of LGETKFs remain close to −1.5 dBZ (Figure 1f), which is the result of over-analyzing the coverage of >40 dBZ echoes (Figure S3 in Supporting Information S1). Some of these differences may be because that the effects of observation-based and the gain-based model-space localization are not identical in practice, and LGETKF and LETKF in JEDI-FV3 version 1.1 using somewhat different vertical analysis grids, and horizontal and vertical localization radii are calculated in combination in LETKF rather than separately as in LGETKF. The differences in analysis mean innovations are much smaller for V_r among the experiments and the analysis mean innovations are much smaller than those of forecasts in earlier and later cycles (Figure 1h). The RMSIs and mean innovations of LGETKF.99 and LGETKF.6 are almost the same for both Z and V_r, suggesting that retaining only 60% of background variance for vertical localization in LGETKF may be sufficient for the current radar DA problem. The similarity in performance between LGETKF.6 and LGETKF.99 could be due to the rather dense radar observations, especially at the mid-to lower levels, so that nearby observations play dominant roles.

The localized probability-matched ensemble mean (LPM, Snook et al., 2020) forecasts of hourly precipitation is calculated for NODA and DA experiments at 1, 2, and 3 hr of forecast and compared with Stage IV hourly precipitation in Figure 2. All DA experiments generally predict a mesoscale convective system with a leading convective line and a trailing weak precipitation region similar to observed (Figures 2a–2c). However, the LPM means overpredict the maximum intensity somewhat, possibly caused by the tendency of high frequency bias of the Thompson microphysics (Skinner et al., 2018). Compared to NODA, the DA experiments better capture the
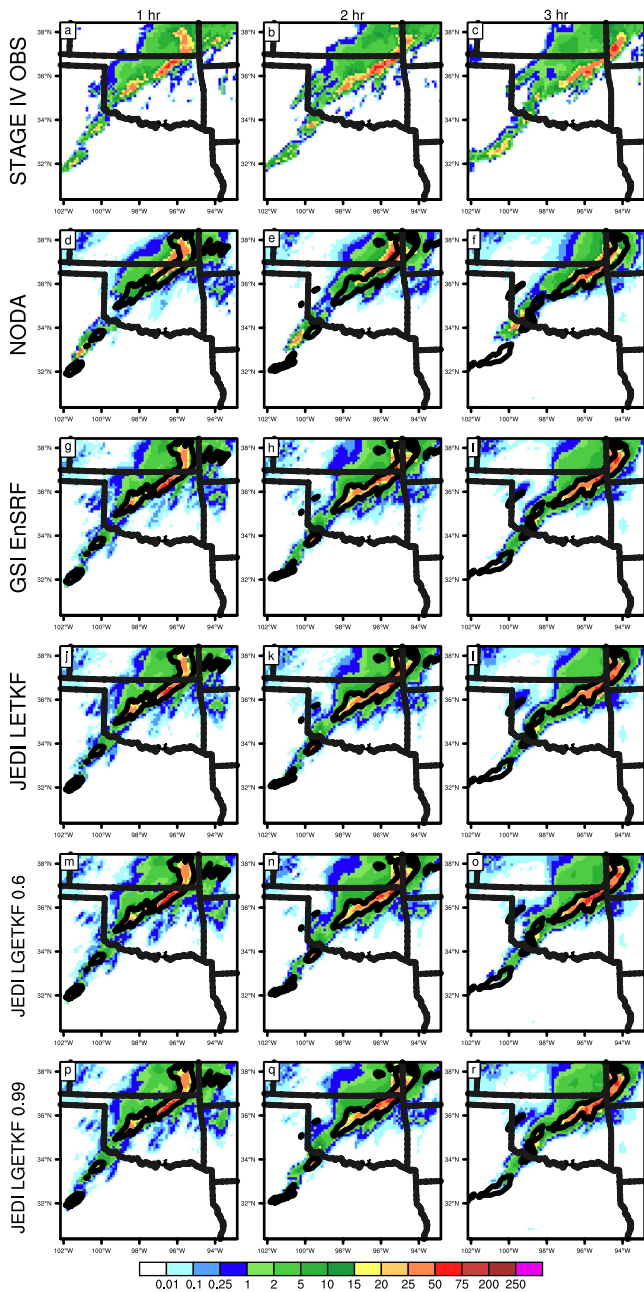
Figure 2. Hourly precipitation (mm) from localized probability-matched mean of 1-hr (left column), 2-hr (middle column) and 3-hr (right column) forecasts from Stage IV observation, EnSRF, LETKF, LGETKF.6, and LGETKF.99. Observed precipitation of 10 mm is contoured in black in the forecasts.

southern portion of the convective line elements as well as the trailing weak precipitation in southern Kansas (Figure 2).

The precipitation forecasts of DA experiments are generally similar but some differences are found in the first forecast hour. LGETKF experiments have more light rainfalls exceeding 1 mm in northwestern Arkansas compared to EnSRF and LETKF (Figures 2g, 2j, 2m, and 2p). The precipitation exceeding 10 mm in western Oklahoma is accurately captured in all DA experiments while a slight eastward displacement in northern Texas is seen in LGETKF.6. Overall, their performances become quite similar in later forecast hours except that LGETKF experiments produce more light precipitation in southern Kansas.

Performance diagrams (Roebber, 2009) relating Probability of Detection (POD), False Alarm Ratio (FAR), Critical Success Index (CSI) and frequency bias of 1/2/3 hr forecast composite reflectivity with 45 dBZ threshold from NODA and DA experiments are shown in Figure 3. Neighborhood skill scores are calculated based on standard contingency table (Table S2 in Supporting Information S1) with a 42-km radius as used in forecast products of the SPC. An overprediction bias is present for all DA experiments in the first 2 hr of forecast, possibly caused by interactions between adjustments from DA and the high frequency bias of the Thompson microphysics as suggested earlier (Skinner et al., 2018). The high biases are much reduced by 3 hr although the overall CSI scores (solid curves labeled 0.4, 0.5, 0.6 and 0.7 are CSI contours) also decreases somewhat (Figure 3c). Compared to NODA (black dots), all DA experiments have clearly higher POD, success ratio and CSI scores for all 3 forecast hours while skill scores for all DA experiments are comparable.

To examine the ability to predict the occurrence of servere weather events, neighborhood maximum ensemble probabilities (NMEP, Ben Bouallègue & Theis, 2014; Schwartz & Sobash, 2017) of 3-hr maximum 2–5 km updraft helicity (UH) exceeding 75 m^2 s^{-2} are compared in Figure 4. The NMEP is calculated with a 42-km neighborhood radius and smoothed with a Gaussian filter with a 81-km Gaussian Kernel (Brooks et al., 1998). For the tornado and hail reports in Texas, the NMEP is less than 40% in NODA (Figure 4a) but the NMEP predicted by the DA experiments are between 40% and 60% (Figures 4b–4e); this is apparently because the parent supercells are more accurately initialized by radar DA (Figure S3 in Supporting Information S1). For the high winds and hail along the southwestern Oklahoma - southwestern Missouri axis, the DA experiments predict NMEP of UH between 60% and 80% with the maximum close to the dense cluster of events in southwestern Missouri (Figures 4b–4e). The NMEPs of DA experiments are very similar except that LGETKFs employing model-space vertical localization diff from EnSRF and LETKF using observation-space vertical localization in that they tend to have a slightly higher probability with the events in Missouri and western Oklahoma.

To assess the computational efficiency of different algorithms in GSI and JEDI, the total elapsed wall time of single EnKF analyses are compared in Figure S4 in Supporting Information S1. When using 40 CPU cores, JEDI LETKF and LGETKF.6 took 15,154 and 5,828 s of walltime, especially for the first public release of JEDI-FV3 (v1.0.0). They took about 30 and 12 times longer than GSI EnSRF, respectively. With the added support for "halo" observation distribution, the computational efficiency of JEDI-FV3 v1.1.2 is improved by a factor of 4–5 compared to v1.0.0. The wall time of LGETKF.99 (3,589 s) is slightly higher than LETKF (3,329 s), but LGETKF.6 (1,001 s) is performed about three times faster than the two experiments in the case of employing 40 cores. By retaining only 60% of variance for
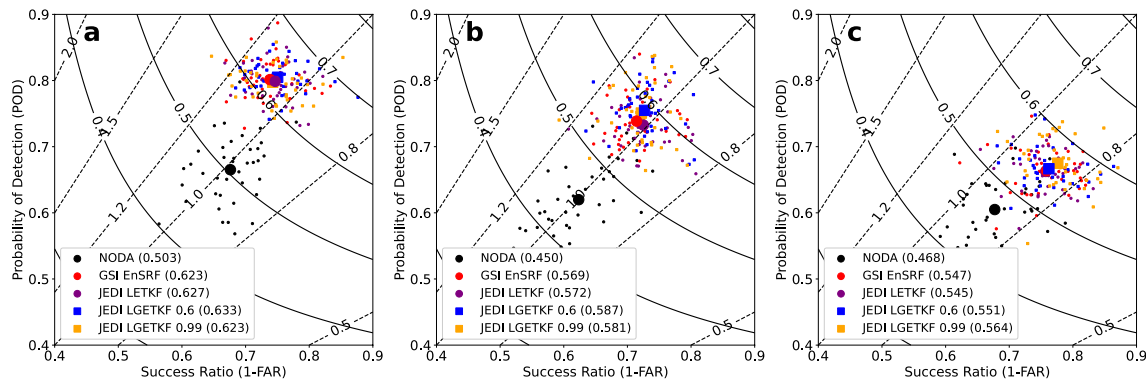
Figure 3. Performance diagrams of composite reflectivity of (a) 1-hr, (b) 2-hr and (c) 3-hr forecast for 45 dBZ thresholds for NODA (black dots), EnSRF (red dots), LETKF(purple dots), LGETKF.6 (blue squares) and LGETKF.99 (orange squares). Smaller symbols indicate scores of individual ensemble members, and larger symbols represent the ensemble mean scores of the experiments.

vertical localization, the cost of LGETKF.6 is reduced by over 70%. When the computational cores are increased from 40 to 225 for JEDI-FV3 v1.1.2, the walltime of LETKF (290 s) is reduced by over 90% while the reduction of LGETKF.99 (1,333 s) is only about 70%. With 225 cores, the computational cost of LETKF is even less than LGETKF.6 (458 s), suggesting that JEDI LETKF has better scaling than JEDI LGETKF. The better scalability of LETKF with increased number of cores used than LGETKF appears to be at least partly because the creation and use of the much larger modulated ensemble and observation innovation calculations for all ensemble members in the latter do not scale as well (Figure S5 in Supporting Information S1). In contrast, GSI takes more time with more cores, mainly because its offline observation prior calculations take much more time using more cores.

5. Summary and Discussion

Direct radar DA capabilities were developed recently within the GSI used by current NWS operational NWP systems. Aiming at the future regional RRFS system, these capabilities are implemented into the JEDI DA system coupled with FV3-LAM and evaluated with the convective storm case of 20 May 2019 over the Southern Plains. Radar radial velocity and reflectivity observations are assimilated every 15 min over a 1-hr DA window using GSI EnSRF, JEDI LETKF, and JEDI LGETKF retaining 60% and 99% of backbround error covariance for vertical localization.

Compared to NODA experiment assimilating no radar data, the assimilation of radar data, regardless of the algorithms used, greatly improves both analyses and forecasts of Z and V_r during the DA window in terms of the RMSIs. Specifically, the storm intensity and location are better predicted in DA experiments, leading to better forecasts of hourly precipitation and updraft helicity. The GSI EnSRF and JEDI LETKF have lower forecast and analyzed RMSIs of Z than JEDI LGETKF during the DA window, but overall all DA experiments have comparable performance for the free forecasts up to 3 hr. Even though JEDI LETKF and LGETKF do not clearly outperform GSI EnSRF in our radar DA study, the parallelization efficiency of JEDI-FV3 v1.1.2 is much better than GSI EnSRF when using over 200 cores; the version benefits from the use of "halo" observation distribution.

The LGETKF DA experiment retaining 60% of background error variance for vertical localization performs similarly as the LGETKF experiment retaining 99% of variance but at only about 1/3 of the computational cost. With JEDI-FV3 v1.1.2 when using 225 (40) cores, the cost of LETKF is much less (more) than LGETKF.6 and GSI EnSRF, suggesting that JEDI LETKF has much better scaling on parallel computers and may be preferred for operational implementation. In short, this study demonstrates, for the first time according to our knowledge, the benefits of directly assimilating radar data within the JEDI ensemble DA framework coupled with the FV3-LAM forecast model. This helps accelerate operational adoption of such capabilities in future regional operational NWP systems at NWS. As a demonstration of new capabilities, this paper is based on testing with a single case; testing with more cases is needed to obtain more robust results. The implementation and testing of radar DA with variational and hybrid methods in JEDI are also ongoing.
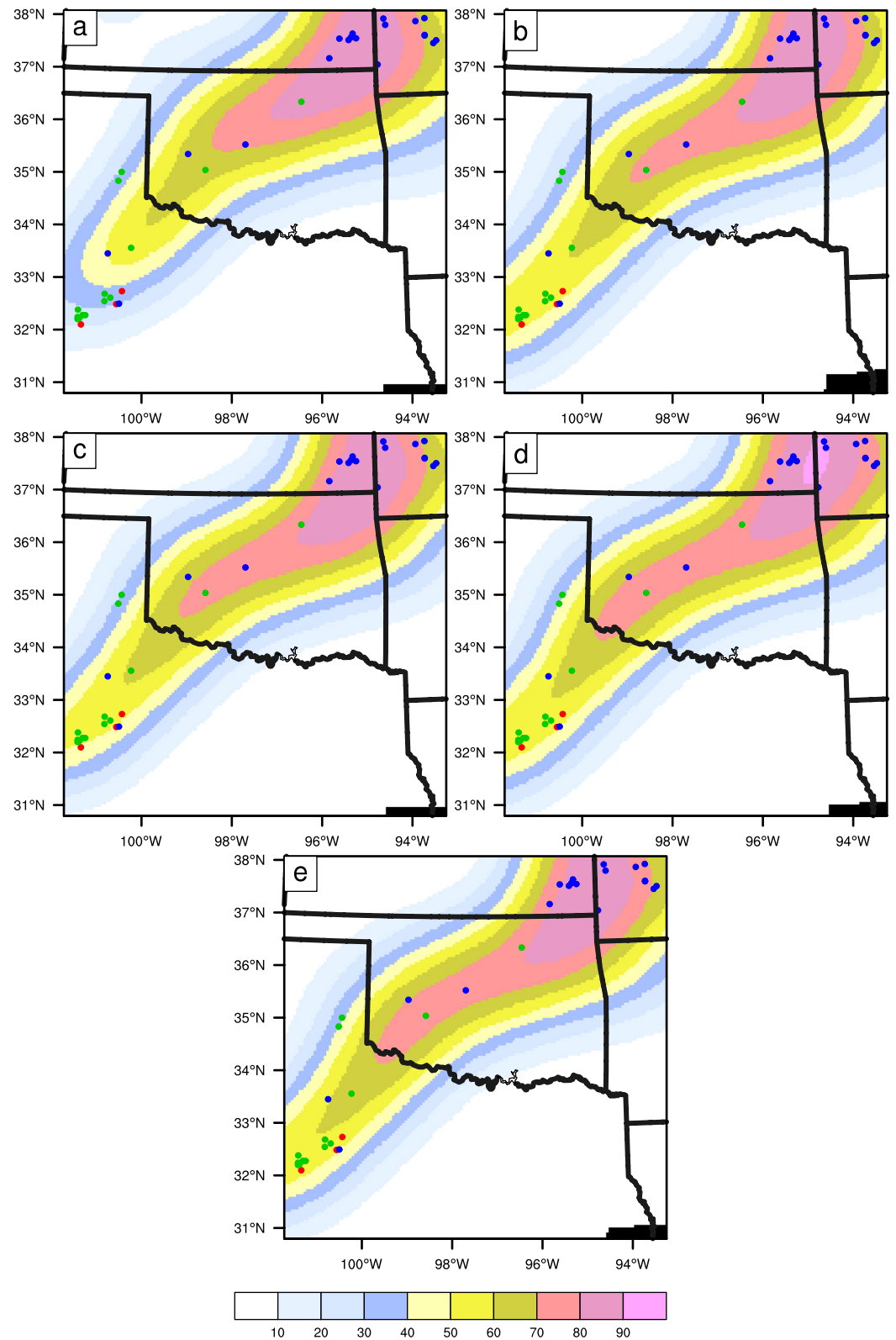
Figure 4. Neighborhood maximum ensemble probability (NMEP) (%) of 3-hr maximum updraft helicity exceeding 75 m^2 s^{-2} for experiments (a) NODA, (b) EnSRF, (c) LETKF, (d) LGETKF.6, and (e) LGETKF.99. The SPC storm reports of high wind, hail, and tornado during the forecast period are represented with blue, green, and red circles, respectively.

Data Availability Statement

The precipitation, reflectivity and updraft helicity data from the FV3-LAM forecasts can be obtained from https://doi.org/10.7910/DVN/ICDC2P. GSI code employed in this study is available at https://github.com/NOAA-EMC/GSI.

References

Baker, N., King, S., Satterfield, E., Ruston, B., Xu, L., Reinecke, P. A., et al. (2022). *An update on the Navy's JEDI-enabled NEPTUNE data assimilation system*. Paper presented at the 10th AMS symposium on the Joint Center for Satellite Data Assimilation (JCSDA) on 102nd American Meteorological Society Annual Meeting 2022, Virtual. Retrieved from https://ams.confex.com/ams/102ANNUAL/meetingapp.cgi/Paper/400203

Ben Bouallègue, Z., & Theis, S. E. (2014). Spatial techniques applied to precipitation ensemble forecasts: From verification results to probabilistic products. *Meteorological Applications*, *21*(4), 922–929. https://doi.org/10.1002/met.1435

Bishop, C. H., Whitaker, J. S., & Lei, L. (2017). Gain form of the ensemble transform Kalman filter and its relevance to satellite data assimilation with model space ensemble covariance localization. *Monthly Weather Review*, *145*(11), 4575–4592. https://doi.org/10.1175/MWR-D-17-0102.1

Black, T. L., Abeles, J. A., Blake, B. T., Jovic, D., Rogers, E., Zhang, X., et al. (2021). A limited area modeling capability for the finite-volume cubed-sphere (FV3) dynamical core and comparison with a global two-way nest. *Journal of Advances in Modeling Earth Systems*, *13*(6). https://doi.org/10.1029/2021MS002483

Brewster, K., Hu, M., Xue, M., & Gao, J. (2005). *Efficient assimilation of radar data at high resolution for short-range numerical weather prediction*. Paper presented at the World Weather Research Program Symposium on Nowcasting and Very Short-Range Forecasting, WSN05, Tolouse, France. Retrieved from https://twister.caps.ou.edu/papers/BrewsterWWRP_Nowcasting.pdf

Brooks, H. E., Kay, M., & Hart, J. (1998). *Objective limits on forecasting skill of rare events*. Paper presented at the 19th conference on severe local storms. American Meteorological Society. Retrieved from https://www.nssl.noaa.gov/users/brooks/public_html/papers/prague2k1.pdf

Chen, L., Liu, C., Jung, Y., Skinner, P., Xue, M., & Kong, R. (2022). Object-based verification of GSI EnKF and hybrid En3DVar radar data assimilation and convection-allowing forecasts within a warn-on-forecast framework. *Weather and Forecasting*, *37*(5), 639–658. https://doi.org/10.1175/WAF-D-20-0180.1

Chen, L., Liu, C., Xue, M., Zhao, G., Kong, R., & Jung, Y. (2021). Use of power transform mixing ratios as hydrometeor control variables for direct assimilation of radar reflectivity in GSI En3DVar and tests with five convective storm cases. *Monthly Weather Review*, *149*(3), 645–659. https://doi.org/10.1175/MWR-D-20-0149.1

Evensen, G. (1994). Sequential data assimilation with a nonlinear quasi-geostrophic model using Monte Carlo methods to forecast error statistics. *Journal of Geophysical Research*, *99*(C5), 10143. https://doi.org/10.1029/94JC00572

Evensen, G. (2003). The ensemble Kalman filter: Theoretical formulation and practical implementation. *Ocean Dynamics*, *53*(4), 343–367. https://doi.org/10.1007/s10236-003-0036-9

Gaspari, G., & Cohn, S. E. (1999). Construction of correlation functions in two and three dimensions. *Quarterly Journal of the Royal Meteorological Society*, *125*(554), 723–757. https://doi.org/10.1002/qj.49712555417

Hamill, T. M., & Snyder, C. (2000). A hybrid ensemble Kalman filter-3D variational analysis scheme. *Monthly Weather Review*, *128*(8), 2905–2919. https://doi.org/10.1175/1520-0493(2000)128<2905:AHEKFV>2.0.CO;2

Harris, L., Chen, X., Putman, W., Zhou, L., & Chen, J. H. (2021). *A scientific description of the GFDL finite-volume cubed-sphere dynamical core*. NOAA Technical Memorandum OAR GFDL 2021-001. https://doi.org/10.25923/6nhs-5897

Heinzeller, D., Firl, G., Bernardet, L., Carson, L., Zhang, M., Schramm, J., et al. (2022). *The common community physics package: Enabling atmospheric physics development for research and operations*. Paper presented at the 31st conference on Weather Analysis and Forecasting (WAF)/27th Conference on Numerical Weather Prediction (NWP) on 102nd American Meteorological Society Annual Meeting 2022. Retrieved from https://ams.confex.com/ams/102ANNUAL/meetingapp.cgi/Paper/390632

Huang, B., Pagowski, M., Trahan, S., Kondragunta, S., Martin, C. R., Tangborn, A., et al. (2022). *Near-real-time global aerosol data assimilation and forecasting using the JEDI-based data assimilation system and the CCPP version of the GEFS-aerosols Model at NOAA/OAR/GSL*. Paper presented at the 12th conference on Transition of Research to Operations on 102nd American Meteorological Society Annual Meeting 2022, Virtual. Retrieved from https://ams.confex.com/ams/102ANNUAL/meetingapp.cgi/Paper/395631

Hunt, B. R., Kostelich, E. J., & Szunyogh, I. (2007). Efficient data assimilation for spatiotemporal chaos: A local ensemble transform Kalman filter. *Physica D: Nonlinear Phenomena*, *230*(1–2), 112–126. https://doi.org/10.1016/j.physd.2006.11.008

Jones, T. A., Skinner, P., Yussouf, N., Knopfmeier, K., Reinhart, A., Wang, X. G., et al. (2020). Assimilation of GOES-16 radiances and retrievals into the warn-on-forecast system. *Monthly Weather Review*, *148*(5), 1829–1859. https://doi.org/10.1175/MWR-D-19-0379.1

Jung, Y., Zhang, G., & Xue, M. (2008). Assimilation of simulated polarimetric radar data for a convective storm using the ensemble Kalman filter. Part I: Observation operators for reflectivity and polarimetric variables. *Monthly Weather Review*, *136*(6), 2228–2245. https://doi.org/10.1175/2007MWR2083.1

Kain, J. S., Xue, M., Coniglio, M. C., Weiss, S. J., Kong, F. Y., Jensen, T. L., et al. (2010). Assessing advances in the assimilation of radar data and other mesoscale observations within a collaborative forecasting-research environment. *Weather and Forecasting*, *25*(5), 1510–1521. https://doi.org/10.1175/2010WAF2222405.1

Kinter, J., Tallapragada, V., & Whitaker, J. S. (2020). *Unified forecast system research-to-operations (UFS-R2O) project proposal*. Retrieved from https://www.weather.gov/media/sti/UFS-R2O-Project-Proposal-Public.pdf

Kleist, D. T., Parrish, D. F., Derber, J. C., Treadon, R., Wu, W.-S., & Lord, S. (2009). Introduction of the GSI into the NCEP global data assimilation system. *Weather and Forecasting*, *24*(6), 1691–1705. https://doi.org/10.1175/2009WAF2222201.1

Labriola, J., Jung, Y., Liu, C., & Xue, M. (2021). Evaluating forecast performance and sensitivity to the GSI EnKF data assimilation configuration for the 28–29 May 2017 mesoscale convective system case. *Weather and Forecasting*, *36*(1), 127–146. https://doi.org/10.1175/WAF-D-20-0071.1

Labriola, J., Snook, N., Jung, Y., & Xue, M. (2020). Evaluating ensemble Kalman filter analyses of severe hailstorms on 8 May 2017 in Colorado: Effects of state variable updating and multimoment microphysics schemes on state variable cross covariances. *Monthly Weather Review*, *148*(6), 2365–2389. https://doi.org/10.1175/MWR-D-19-0300.1

Lei, L., Whitaker, J. S., & Bishop, C. (2018). Improving assimilation of radiance observations by implementing model space localization in an ensemble Kalman filter. *Journal of Advances in Modeling Earth Systems*, *10*(12), 3221–3232. https://doi.org/10.1029/2018MS001468

Li, H., Liu, C., Xue, M., Park, J., Chen, L., Jung, Y., et al. (2022). Use of power transform total number concentration as control variable for direct assimilation of radar reflectivity in GSI En3DVar and tests with six convective storms cases. *Monthly Weather Review*, *150*(4), 821–842. https://doi.org/10.1175/MWR-D-21-0041.1

Lin, S. J. (2004). A "vertically Lagrangian" finite-volume dynamical core for global models. *Monthly Weather Review*, *132*(10), 2293–2307. https://doi.org/10.1175/1520-0493(2004)132<2293:AVLFDC>2.0.CO;2

Liu, C., Li, H., Xue, M., Jung, Y., Park, J., Chen, L., et al. (2022). Use of a reflectivity operator based on double-moment Thompson microphysics for direct assimilation of radar reflectivity in GSI-based hybrid En3DVar. *Monthly Weather Review*, *150*(4), 907–926. https://doi.org/10.1175/MWR-D-21-0040.1

Liu, Z., Snyder, C., Guerrette, J. J., Jung, B.-J., Ban, J., Vahl, S., et al. (2022). Data assimilation for the model for prediction across scales–atmosphere with the Joint Effort for Data Assimilation Integration (JEDI-MPAS 1.0. 0): EnVar implementation and evaluation. *Geoscientific Model Development*, *15*(20), 7859–7878. https://doi.org/10.5194/gmd-15-7859-2022

Luo, J. Y., Li, H., Xue, M., & Zhu, Y. J. (2022). Direct assimilation of radar reflectivity data using ensemble Kalman filter based on a two-moment microphysics scheme for the analysis and forecast of Typhoon Lekima (2019). *Remote Sensing*, *14*(16), 3987. https://doi.org/10.3390/rs14163987

Miyoshi, T., & Yamane, S. (2007). Local ensemble transform Kalman filtering with an AGCM at a T159/L48 resolution. *Monthly Weather Review*, *135*(11), 3841–3861. https://doi.org/10.1175/2007MWR1873.1

Putman, W. M., & Lin, S.-J. (2007). Finite-volume transport on various cubed-sphere grids. *Journal of Computational Physics*, *227*(1), 55–78. https://doi.org/10.1016/j.jcp.2007.07.022

Roebber, P. J. (2009). Visualizing multiple measures of forecast quality. *Weather and Forecasting*, *24*(2), 601–608. https://doi.org/10.1175/2008WAF2222159.1

Schneider, T., DeLuca, C., Jasko, S., Rakesh, B., Archambault, H., Bua, B., et al. (2017). *Unified forecast system communication & outreach plan*. Retrieved from https://ufscommunity.org/wp-content/uploads/2019/10/20171221_Unified_Forecast_System_CommunicationOutreach_Plan.pdf

Schwartz, C. S., & Sobash, R. A. (2017). Generating probabilistic forecasts from convection-allowing ensembles using neighborhood approaches: A review and recommendations. *Monthly Weather Review*, *145*(9), 3397–3418. https://doi.org/10.1175/MWR-D-16-0400.1

Skamarock, W. C., Klemp, J. B., Duda, M. G., Fowler, L. D., Park, S. H., & Ringler, T. D. (2012). A multiscale nonhydrostatic atmospheric model using Centroidal Voronoi Tesselations and C-grid staggering. *Monthly Weather Review*, *140*(9), 3090–3105. https://doi.org/10.1175/MWR-D-11-00215.1

Skinner, P. S., Wheatley, D. M., Knopfmeier, K. H., Reinhart, A. E., Choate, J. J., Jones, T. A., et al. (2018). Object-based verification of a prototype Warn-on-Forecast system. *Weather and Forecasting*, *33*(5), 1225–1250. https://doi.org/10.1175/WAF-D-18-0020.1

Smith, T. M., Lakshmanan, V., Stumpf, G. J., Ortega, K. L., Hondl, K., Cooper, K., et al. (2016). Multi-radar multi-sensor (MRMS) severe weather and aviation products: Initial operating capabilities. *Bulletin of the American Meteorological Society*, *97*(9), 1617–1630. https://doi.org/10.1175/BAMS-D-14-00173.1

Snook, N., Kong, F. Y., Clark, A., Roberts, B., Brewster, K. A., & Xue, M. (2020). Comparison and verification of point-wise and patch-wise localized probability-matched mean algorithms for ensemble consensus precipitation forecasts. *Geophysical Research Letters*, *47*(12). https://doi.org/10.1029/2020GL087839

Snyder, C., & Zhang, F. Q. (2003). Assimilation of simulated Doppler radar observations with an ensemble Kalman filter. *Monthly Weather Review*, *131*(8), 1663–1677. https://doi.org/10.1175//2555.1

Stensrud, D. J., Wicker, L. J., Xue, M., Dawson, D. T., Yussouf, N., Wheatley, D. M., et al. (2013). Progress and challenges with warn-on-forecast. *Atmospheric Research*, *123*, 2–16. https://doi.org/10.1016/j.atmosres.2012.04.004

Stensrud, D. J., Xue, M., Wicker, L. J., Kelleher, K. E., Foster, M. P., Schaefer, J. T., et al. (2009). Convective-scale warn-on-forecast system: A vision for 2020. *Bulletin of the American Meteorological Society*, *90*(10), 1487–1500. https://doi.org/10.1175/2009BAMS2795.1

Sun, J. Z., Xue, M., Wilson, J. W., Zawadzki, I., Ballard, S. P., Onvlee-Hooimeyer, J., et al. (2014). Use of NWP for nowcasting convective precipitation: Recent progress and challenges. *Bulletin of the American Meteorological Society*, *95*(3), 409–426. https://doi.org/10.1175/BAMS-D-11-00263.1

Thompson, G., Field, P. R., Rasmussen, R. M., & Hall, W. D. (2008). Explicit forecasts of winter precipitation using an improved bulk microphysics scheme. Part II: Implementation of a new snow parameterization. *Monthly Weather Review*, *136*(12), 5095–5115. https://doi.org/10.1175/2008MWR2387.1

Tong, C. C., Jung, Y., Xue, M., & Liu, C. (2020). Direct assimilation of radar data with ensemble Kalman filter and hybrid ensemble-variational method in the National Weather Service Operational Data Assimilation System GSI for the stand-alone regional FV3 model at a convection-allowing resolution. *Geophysical Research Letters*, *47*(19). https://doi.org/10.1029/2020GL090179

Tong, M., & Xue, M. (2005). Ensemble Kalman filter assimilation of Doppler radar data with a compressible nonhydrostatic model: OSS experiments. *Monthly Weather Review*, *133*(7), 1789–1807. https://doi.org/10.1175/MWR2898.1

Trémolet, Y., & Auligné, T. (2020). The Joint Effort for Data Assimilation Integration (JEDI). *JCSDA Quarterly Newsletter*, *66*. https://doi.org/10.25923/rb19-0q26

UFS Development Team. (2022). Unified forecast system (UFS) short-range weather (SRW) application (version v2.0.0). *Zenodo*. https://doi.org/10.5281/zenodo.6505854

Wheatley, D. M., Knopfmeier, K. H., Jones, T. A., & Creager, G. J. (2015). Storm-scale data assimilation and ensemble forecasting with the NSSL experimental warn-on-forecast system. Part I: Radar data experiments. *Weather and Forecasting*, *30*(6), 1795–1817. https://doi.org/10.1175/WAF-D-15-0043.1

Whitaker, J. S., & Hamill, T. M. (2002). Ensemble data assimilation without perturbed observations. *Monthly Weather Review*, *130*(7), 1913–1924. https://doi.org/10.1175/1520-0493(2002)130<1913:EDAWPO>2.0.CO;2

Whitaker, J. S., & Hamill, T. M. (2012). Evaluating methods to account for system errors in ensemble data assimilation. *Monthly Weather Review*, *140*(9), 3078–3089. https://doi.org/10.1175/MWR-D-11-00276.1

Xue, M., Tong, M. J., & Droegemeier, K. K. (2006). An OSSE framework based on the ensemble square root Kalman filter for evaluating the impact of data from radar networks on thunderstorm analysis and forecasting. *Journal of Atmospheric and Oceanic Technology*, *23*(1), 46–66. https://doi.org/10.1175/JTECH1835.1